Skeletal dosimetry for external exposures to photons based on μCT images of spongiosa: Consideration of voxel resolution, cluster size and medullary bone surfaces

R Kramer [1], H J Khoury [1], J W Vieira [2, 3] and K A Robson Brown [4]

[1] Departamento de Energia Nuclear, Universidade Federal de Pernambuco, Av. Prof. Luiz Freire 1000, Cidade Universitária, CEP 50740-540, Recife, PE, Brazil

[2] Centro Federal de Educação Tecnológica de Pernambuco, Recife, PE, Brazil

[3] Escola Politécnica, UPE, Recife, PE, Brazil

[4] Imaging Laboratory, Department of Archaeology and Anthropology, University of Bristol, Bristol, UK

Statement of provenance:
'This is an author-created, un-copyedited version of an article accepted for publication in Medical Physics. The American Association of Physicists in Medicine is not responsible for any errors or omissions in this version of the manuscript or any version derived from it. The definitive publisher authenticated version is available at DOI: 10.1118/1.3242266. '

Abstract

Skeletal dosimetry based on μCT images of trabecular bone has recently been introduced to calculate the red bone marrow (RBM) and the bone surface cells (BSC) equivalent doses in human phantoms for external exposure to photons. In order to use the μCT images for skeletal dosimetry, spongiosa voxels in the skeletons were replaced at run time by so-called micro matrices, which have exactly the size of a spongiosa voxel and contain segmented trabecular bone and marrow micro voxels. A cluster (= parallelepiped) of 2x2x2=8 micro matrices was used systematically and periodically throughout the spongiosa volume during the radiation transport calculation. Systematic means that when a particle leaves a spongiosa voxel to enter into a neighbouring spongiosa voxel, then the next micro matrix in the cluster will be used. Periodical means that if the particle travels through more than two spongiosa voxels in a row, then the cluster will be repeated. Based on the bone samples available at the time, clusters of up to 3x3x3=27 micro matrices were studied. While for a given trabecular bone volume fraction the whole-body RBM equivalent dose showed converging results for cluster sizes between 8 and 27 micro matrices, this was not the case for the BSC equivalent dose. The BSC equivalent dose seemed to be very sensitive to the number, form and thickness of the trabeculae. In addition, the cluster size and/or the micro voxel resolution were considered to be possible causes for the differences observed. In order to resolve this problem, this study used a bone sample large enough to extract clusters containing up to 8x8x8=512 micro matrices and which was scanned with two different voxel resolutions. Taking into account a recent proposal, this investigation also calculated the BSC equivalent dose on medullary surfaces of cortical bone in the arm and leg bones. The results showed 1) that different voxel resolutions have no effect on the RBM equivalent dose, but do influence the BSC equivalent dose due to voxel effects by up to 5% for incident photon energies up to 200 keV, 2) that the whole-body BSC equivalent dose calculated with a cluster with 2x2x2=8 micro matrices is consistent with results received with clusters of up to 8x8x8=512 micro matrices and 3) that for external whole-body exposure the inclusion of the BSC on medullary surfaces of cortical bone has a negligible effect on the whole-body BSC equivalent dose.

I INTRODUCTION

A. Skeletal tissues at risk

In the skeleton, two soft tissues are at risk when ionising radiation penetrates the human body: the haematopoietic stem cells of the marrow, called "red bone marrow" (RBM), and the osteogenic cells on the endosteal surfaces, called "bone surface cells" (BSC) or bone endosteum. The BSC represent the part of the marrow volume that is located within a distance of 10 μm from the surfaces of trabecular bone, of cortical bone neighbouring spongiosa and of medullary cortical bone, whereas the RBM occupies a part of the remaining trabecular marrow volume given by the cellularity factor[1, 2]. Spongiosa represents the trabecular bone structure filled with soft tissue.

B. Skeletal dosimetry based on μCT images of spongiosa

W.Bolch and his research group from the University of Florida were the first to use μCT images of trabecular bone for the purposes of dosimetry[3-9]. In these studies, samples from various bone sites of human skeletons were scanned by μCT or NMR, the resulting images were segmented into trabecular bone and marrow, and then introduced first into the EGS4 (Electron-Gamma-Shower, version 4) Monte Carlo (MC) code[10], and later into the EGSnrc (Electron-Gamma-Shower, version *N*ational *R*esearch *C*ouncil, Canada) MC code [11], employing a special algorithm called PIRT ("paired-image radiation transport"). In the PIRT method particles are transported through a "macro" matrix with a voxel size of some hundred μm, representing spongiosa, cortical bone and surrounding soft tissues, and at the same time through a "micro" matrix with cubic voxel resolutions of 30 μm and larger, representing the micro structure of spongiosa with segmented volumes of marrow and trabecular bone.

For external exposure to photons, skeletal dosimetry for a complete adult human skeleton based on μCT images of spongiosa has recently been introduced by authors of this study [12, 13]. Clusters of so-called 'micro matrices' have been extracted from μCT images of adult human spongiosa and introduced into the spongiosa voxels of two adult human voxel phantoms at run time of MC calculations with the EGSnrc code[11, 14-16] to determine the whole-body equivalent doses to the RBM and the BSC as a function of parameters like the donor of the bone, the bone site, the segmentation method, the number of micro matrices in the cluster, etc. A micro matrix is a 3D μCT image of trabecular bone with exactly the size of a voxel of the spongiosa segmented in the skeleton of a phantom. A cluster is a parallelepiped of spongiosa volume containing a certain number of micro matrices extracted from the μCT image of a bone sample. At run time, when a particle enters a spongiosa voxel, radiation transport is transferred to the first micro matrix in the cluster. If the next voxel is again a spongiosa voxel, then the second micro matrix in the cluster is used, etc. If all micro matrices of the cluster have been used and the particle continues to travel still in spongiosa, then the cluster is repeated. This *s*ystematic and *p*eriodic use of the cluster throughout the spongiosa volume was called the SP cluster method. The bone samples available at the time allowed for the extraction of up to 3x3x3=27 micro matrices. For a given trabecular bone volume fraction (TBVF) of the bone sample, the RBM equivalent dose showed consistent results for clusters with 8 to 27 micro matrices, whereas the BSC equivalent dose showed differences indicating that clusters with a greater number of micro matrices were probably needed to achieve consistent results. At the same time it was realized that the voxel resolution (= voxel size) used during scanning of the bone samples may also influence the RBM and the BSC equivalent doses. To resolve this problem, one would have to scan at least one bone sample with two different voxel resolutions, a procedure not usually undertaken in μCT imaging. Finally, as our earlier studies did not consider BSC on medullary surfaces of cortical bone it was decided to include this part of the BSC to see its impact on the whole-body BSC equivalent dose.

C. The purpose of this study

In order to complement the earlier investigations on skeletal dosimetry for external exposure to photons based on μCT images of human spongiosa, this study addresses the following unresolved questions employing μCT images now available from a larger bone sample scanned at two different voxel resolutions:

Does the voxel resolution of the μCT images influence the RBM and the BSC equivalent doses?

Is a coherent spongiosa volume made of 8 micro matrices sufficient to guarantee consistent results for the BSC equivalent dose? In other words, does the BSC equivalent dose still change when the number of micro matrices in the cluster becomes greater than 8?

What is the effect on the BSC equivalent dose if BSC on medullary surfaces of cortical bone are included in the calculations?

II MATERIALS AND METHODS

The methodology for describing the MAX06 (*M*ale *A*dult vo*X*el, version 06) and the FAX06 (*F*emale *A*dult vo*X*el, version 06) phantoms, the processing of the μCT images, the application of the 8 SP (***8*** micro matrices ***s***ystematically and ***p***eriodically used) cluster method and the use of the EGSnrc MC code have all been presented in previous papers published by the dosimetry research group at the University of Pernambuco [12, 13, 17] and have been briefly summarized in chapter I-B. The current chapter, therefore, will focus on the new developments, i.e. the acquisition and processing of μCT images of a larger bone sample scanned with two different resolutions, the extraction of clusters with up to 512 micro matrices from the images and the introduction of the algorithm for medullary bone surfaces.

A. Extraction of the same spongiosa volume based on two different resolutions

A first lumbar vertebra (L1), approximately 3.2 cm x 3.5 cm x 2.7 cm in size, was scanned with a μCT scanner Skyscan 1172 (Skyscan Corporation, 2630 Aartselaar, Belgium) with 80 kVp (100 μA) at 30 μm and 60 μm resolution at the Imaging Laboratory for Anthropology of the University of Bristol, UK. The skeleton, a donation to medical science, came from an anatomical teaching collection. The subject was a female adult of 30 years, height of 1.49 m and unknown weight. The 30 μm scan resulted in 1068 images with 1984 x 1984 pixels each, whereas the 60 μm scan produced 534 images with 992 x 992 pixels each.

The SP cluster method requires the extraction of a parallelepiped with at least 8 micro matrices from the spongiosa volume, with each of the micro matrices having a cubic size of 1.2 mm, because this is the voxel size used in the adult human phantoms MAX06 and FAX06 [17]. In order to make sure that one investigates only the effect of the voxel resolution, it is crucial to extract the 30 μm-based and the 60 μm-based parallelepipeds at exactly the same position within the spongiosa volumes of the two image sets. This ensures that two parallelepipeds with identical trabecular bone structure are extracted. Verifying the images slice by slice it was found by visual inspection that identical first images of trabecular bone appeared in image No. 192 for 30 μm and in image No. 96 for 60 μm resolution, respectively.

Using images 192 and 96 as reference slices, two 9.6 mm cubes were extracted at the same location in the two spongiosa volumes, thereby extracting exactly the same trabecular bone structure from the two image sets. The segmentation procedure followed the published protocol [12, 13]. After the removal of

noise with a median filter (kernel size 3x3x3), the images were segmented into trabecular bone and marrow using a histogram-based threshold function [18].
Although representing the same trabecular bone structure, visual inspection showed that the segmented images for the two voxel resolutions were not identical with respect to the number, the form and the thickness of the trabeculae. The visualization of differences between the trabecular bone structures of the two cubes is shown in 2D representations in figures 1, 2 and 3.

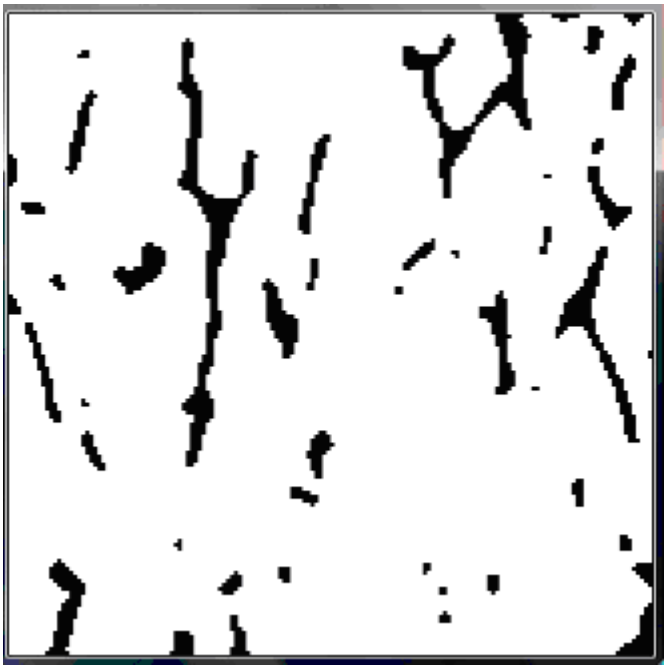

Figure 1. First 2-dimensional image of the 9.6 mm cube scanned at 60 μm resolution

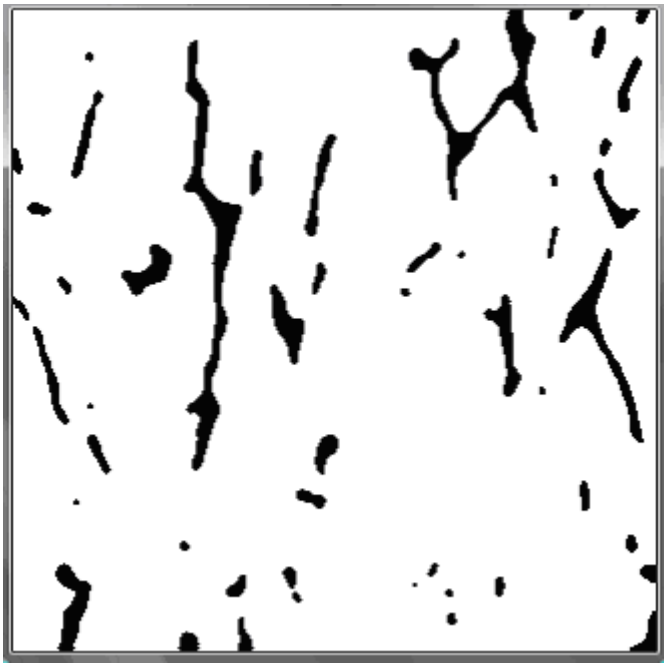

Figure 2. First 2-dimensional image of the 9.6 mm cube scanned at 30 μm resolution

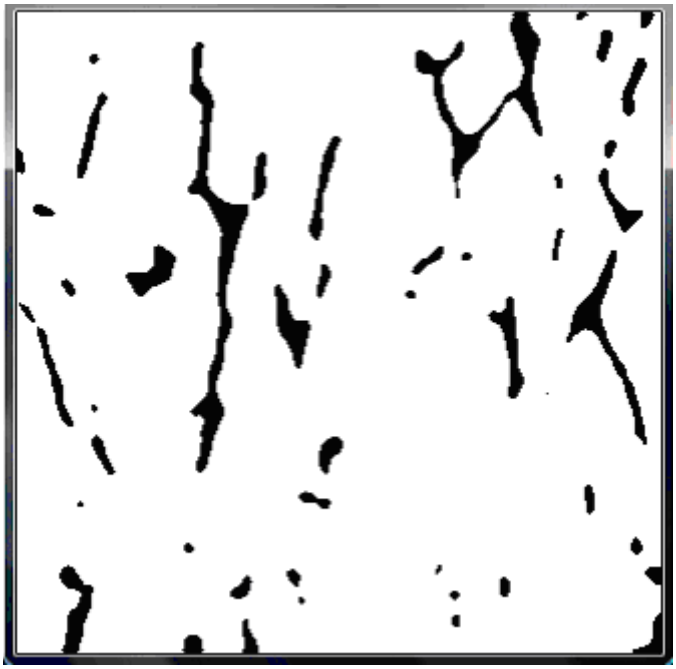

Figure 3. Second 2-dimensional image of the 9.6 mm cube scanned at 30 μm resolution

Figure 1 shows the first of 160 2D images of the 9.6 mm cube scanned at 60 μm resolution, whereas figures 2 and 3 show the first and the second of 320 2D images, respectively, of the 9.6 mm cube scanned at 30 μm resolution. Trabecular bone is represented by the black areas, whereas marrow is represented by the white areas. The pixel-like trabecular bone surface can clearly be seen. Increasing the resolution from 60 to 30 μm means that every 60 μm voxel will then be represented by eight 30 μm voxels, thereby allowing for a finer representation of the trabecular bone surface. Figures 2 and 3 show this effect, where a smoother trabecular bone surface can be seen compared to figure 1. One can see that the trabecular bone structures in figure 1 on the one hand and in figures 2 plus 3 on the other hand are not identical. For example, a 60 μm scanned and segmented bone pixel, located at the surface of trabecular bone, can become four segmented bone pixels or three segmented bone and one segmented marrow pixel if later scanned with 30 μm resolution. The same effect will be observed for a 60 μm-scanned and segmented marrow pixel located at the surface of the cavity volume. In other words, due to voxel effects, which have been discussed earlier [12], a 60 μm surface bone or marrow voxel will not always correspond to eight 30 μm surface bone or marrow voxels, respectively. The differences between the trabecular bone structures (= number, form and thickness of the trabeculae) are also reflected by the TBVFs. These, were found to be 7.93% for the 30 μm-based cube and 8.20% for the 60 μm-based 9.6 mm cube, despite representing to the same trabecular bone volume.

B. Clusters with different numbers of micro matrices

The BSC algorithm was introduced in the second study on skeletal dosimetry based on μCT images of spongiosa [13], but the bone samples available at the time were too small to allow for a significant increase of the number of micro matrices in the cluster. With the lumbar vertebra used in this study this limitation could be overcome. Taking into account a cubic size of 1.2 mm for the micro matrices in a cluster, a 9.6 mm cube of spongiosa then allows for an extraction of parallelepipeds with up to 8x8x8 micro matrices. Taking the center of the 9.6 mm cube as the center for the clusters, parallelepipeds with 2x2x2, 3x3x3, 4x4x4, 5x5x5, 6x6x6, 7x7x7 and 8x8x8 micro matrices were extracted from the 60 μm-based cube. Table 1 shows the cluster sizes and the TBVFs as a function of the number of micro matrices in the cluster based on the 60 μm-scanned CT images.

Table 1. Cluster sizes, number of micro matrices and trabecular bone volume fractions for clusters with 8 to 512 micro matrices scanned at 60 μm voxel resolution

Cluster	Number of micro matrices	Cluster size kB	60 μm TBVF %
2x2x2	8	257	8.32
3x3x3	27	865	8.67
4x4x4	64	2050	8.19
5x5x5	125	4004	7.78
6x6x6	216	6919	7.99
7x7x7	343	10987	8.12
8x8x8	512	16400	8.20

C. Medullary cortical bone surfaces

BSC located on cortical bone surfaces has already been taken account of in earlier calculations for those cortical bone surfaces which are in contact with the marrow cavities of trabecular bone [12]. However, it has recently been suggested that in addition to cortical bone surfaces adjacent to spongiosa, medullary cortical bone surfaces of arm and leg bones should also be taken into account when determining the equivalent dose to the BSC [19]. Medullary cortical bone surfaces form the walls of large, tube-like cavities in the upper and lower arm and leg bones, also called "long bones", filled for adults only with yellow bone marrow (YBM), which is not considered to be a target tissue for skeletal dosimetry.

The BSC algorithm, developed and applied earlier [13], was extended in this study to medullary cortical bone surfaces. At run time, the Monte Carlo code first determines the medullary BSC volume for a 10 μm layer thickness in those YBM macro voxels which have cortical bone voxels as neighbours. During the Monte Carlo calculation, the energy to be deposited in an YBM voxel is divided between the BSC and the remaining YBM volumes according to the linear path length fraction within the corresponding sub-volume for the electron step under consideration.

III. RESULTS AND DISCUSSION

The calculations were executed using the SP cluster method based on the EGSnrc MC code and applied to the FAX06 and the MAX06 phantoms for whole body external exposures with parallel photon fields with anterior-posterior (AP) and posterior-anterior (PA) incidence with energies between 10 keV and 10 MeV. The minimal cortical bone thickness in the skeletons is 1.2 mm. This implies that electrons moving in regions outside the skeleton must have a kinetic energy of at least 550 keV in order to enter a spongiosa voxel after having passed through the cortical layer. Thus, cut-off energies were set to 2 keV for photons, 550 keV for electrons in tissues outside the skeleton and 5 keV for electrons in the skeletal tissues. All EGSnrc transport parameters and cross section options were left at their default values, which are set to achieve the best accuracy EGSnrc is capable of. The numbers of incident photons varied between 5 and 40 million in order to arrive at the coefficients of variation (C.V.), i.e. the statistical errors, for the whole body RBM and the BSC equivalent doses shown in table 2. The statistical errors are generally below 1%, except for very low incident photon energies. The results are presented as conversion coefficients (CCs) between equivalent dose and air kerma free-in-air. As was found in the first two publications on skeletal dosimetry based on μCT images of

spongiosa [12, 13], apart from differences with respect to absolute values the basic characteristics of the results are the same for the MAX06 and the FAX06 phantoms. Therefore, in order not to inflate the scope of this study unnecessarily, the graphical results presented below illustrate only one of the two phantoms for AP or PA incidence.

Table 2. Statistical errors, expressed as coefficients of variation for RBM and BSC equivalent doses for all calculations shown in this study

Incident energy	C.V. RBM	C.V. BSC
	%	%
15 keV	3.5	-
20 keV	0.6	1.7
30 keV-10 MeV	< 0.5	< 0.8

A. Micro voxel resolution

In section II A it was shown that representing the same spongiosa volume with segmented μCT images based on different voxel resolutions is possible only if one accepts at least small differences between the trabecular bone structures (= number, form and thickness of the trabeculae) of the two images, due to the voxel effects involved in the segmentation process. For the calculations presented here, clusters of 2x2x2 = 8 micro matrices have been extracted from the centers of the two 9.6 mm cubes mentioned above. The original TBVFs were 8.26% and 8.32% for 30 μm and 60 μm resolutions, respectively, i.e. both clusters had basically the same TBVF.

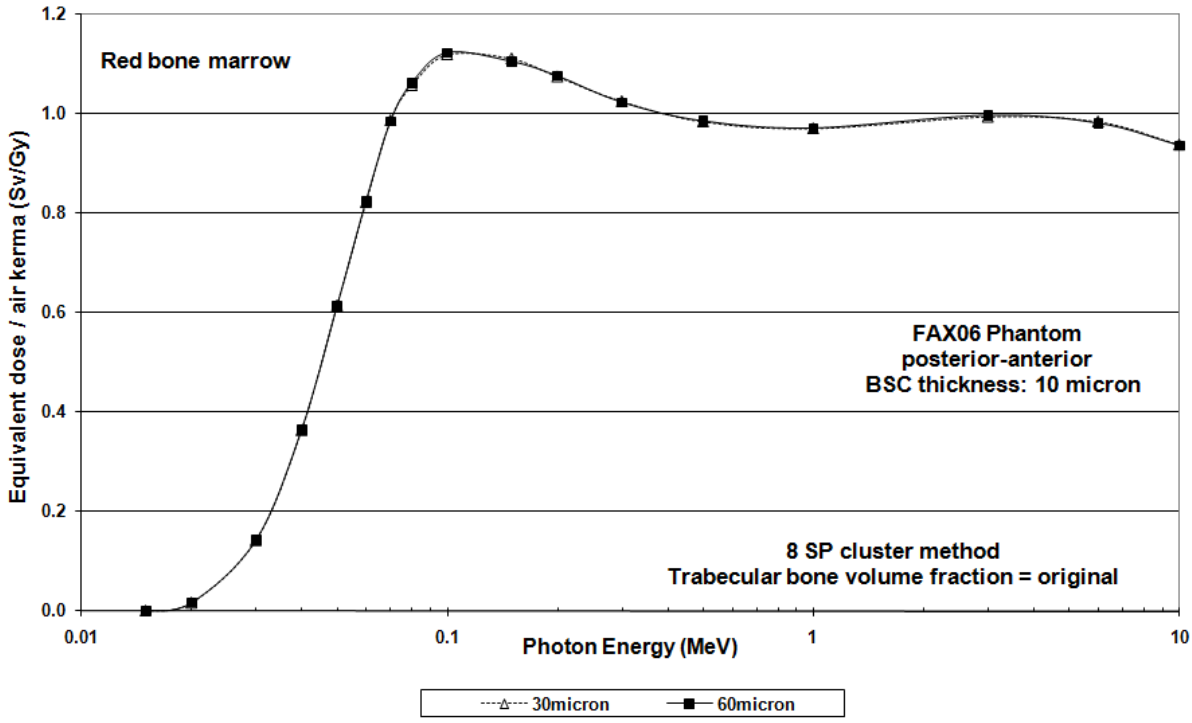

Figure 4. Red bone marrow equivalent dose conversion coefficients for the FAX06 phantom using the same bone sample scanned at 30 and 60 μm resolution for posterior-anterior incidence and original trabecular bone volume fractions.

Table 3 Ratios between red bone marrow equivalent dose conversion coefficients for 30 and 60 μm voxel resolutions used for the scanning of the same bone sample

E (MeV)	RBM 30/60 FAX06 AP	RBM 30/60 FAX06 PA	RBM 30/60 MAX06 AP	RBM 30/60 MAX06 PA
0.015	1.000	1.000	1.000	1.000
0.02	0.993	0.994	1.000	0.993
0.03	0.997	0.998	0.995	1.008
0.04	0.996	0.999	0.998	0.994
0.05	1.000	1.004	1.005	1.003
0.06	0.998	0.998	0.998	0.999
0.07	1.000	1.004	1.002	0.995
0.08	0.997	0.996	0.998	0.997
0.1	1.001	0.998	1.001	1.002
0.15	1.002	1.007	0.996	0.998
0.2	1.000	1.000	0.998	0.998
0.3	0.998	1.003	0.999	0.998
0.5	1.001	1.000	1.000	0.997
1.0	0.995	1.000	0.996	1.000
3.0	0.997	0.998	1.001	1.005
6.0	1.006	1.004	0.992	1.001
10.0	0.991	1.003	1.007	1.005

Figure 4 shows RBM equivalent dose CCs for the FAX06 phantom for PA incidence as a function of the incident photon energy calculated with the 8 SP cluster method for 30 μm and 60 μm resolutions. Differences between the two CCs are very small, almost negligible. For AP incidence and for the MAX06 phantom similar small differences between the CCs for different voxel resolutions were also found. Table 3 presents ratios between RBM equivalent dose CCs for 30 μm and 60 μm resolution for both phantoms and both directions of incidence. All ratios show differences of less than 1%, i.e. that they are within the range of the combined statistical errors according to table 2. Different voxel resolutions lead to slightly different trabecular bone structures in the segmented images of the same bone sample as shown above, which in turn causes different fluxes of photoelectrons released by photons in the trabeculae. The ranges of these trabecular photoelectrons are small compared to the diameters of the marrow cavities and the differences between the 30 μm and the 60 μm fluxes are also small, because, as figures 1-3 have shown, the two images are very much alike. Consequently, the differences between the 30 μm-scanned and the 60 μm-scanned images have a negligible effect on the RBM equivalent dose.

Corresponding results are shown in figure 5 and table 4 for the BSC. Although still small, the differences between the CCs for the two resolutions can clearly be seen in figure 6. In table 4, those differences which exceed the range of the combined statistical errors are shown as bold, italic numbers. The greatest difference found is 4.6%, and all statistically relevant differences occur for incident photon energies below 200 keV. Photoelectrons, primarily from trabecular bone, contribute strongly to the total BSC equivalent dose in this energy range. Small differences between the trabecular bone structures for the two resolutions cause differences in the photoelectron fluxes, which in turn influence the BSC equivalent doses because the BSC are located at a distance of only 10 μm from the trabecular bone surface. For energies above 200 keV, secondary electrons from trabecular bone are mostly Compton and later additionally pair production electrons, whose fluxes are hardly influenced by the small differences between the trabecular bone structures of the two μCT images. Consequently, the differences shown in table 4 for incident photon energies above 200 keV are within the range of the combined statistical errors. In contrast to the RBM, the BSC equivalent dose may increase by up to almost 5% for low incident photons energies when the voxel resolution of the μCT images increases from 60 to 30 μm.

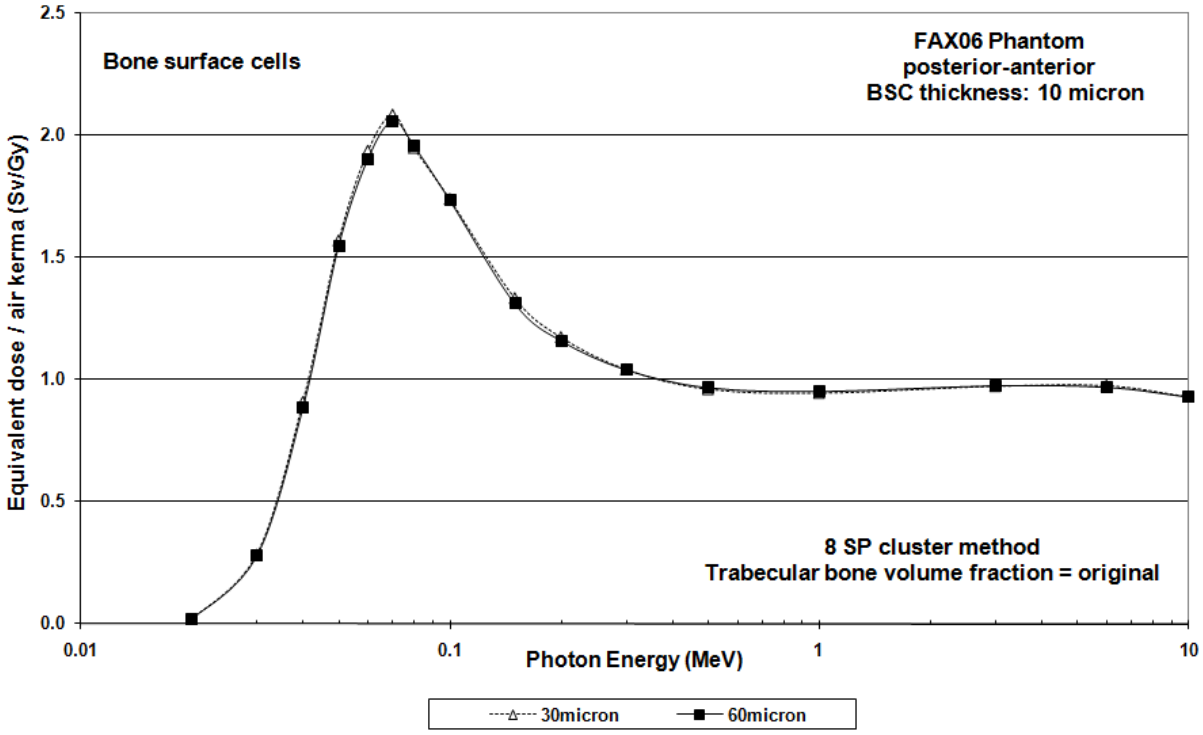

Figure 5. Bone surface cells equivalent dose conversion coefficients for the FAX06 phantom using the same bone sample scanned at 30 and 60 μm resolution for posterior-anterior incidence and original trabecular bone volume fractions

Table 4. Ratios between bone surface cells equivalent dose conversion coefficients for 30 and 60 μm voxel resolutions used for the scanning of the same bone sample

E (MeV)	BSC 30/60 FAX06 AP	BSC 30/60 FAX06 PA	BSC 30/60 MAX06 AP	BSC 30/60 MAX06 PA
0.02	1.029	1.014	1.036	1.013
0.03	***1.041***	***1.029***	***1.046***	***1.020***
0.04	***1.032***	***1.029***	***1.041***	***1.039***
0.05	***1.023***	1.015	***1.022***	***1.040***
0.06	1.008	***1.018***	***1.019***	***1.030***
0.07	1.004	1.012	1.004	***1.024***
0.08	***1.017***	0.995	***1.023***	1.010
0.1	0.990	1.003	1.005	1.005
0.15	0.995	***1.018***	0.995	0.995
0.2	0.995	1.013	1.005	1.022
0.3	1.000	1.003	0.996	0.989
0.5	1.016	0.994	1.010	0.992
1.0	1.002	0.993	1.006	0.998
3.0	0.997	0.999	0.999	1.002
6.0	0.998	1.008	0.999	0.992
10.0	0.994	1.002	1.012	1.003

B. Number of micro matrices

Previous investigations into skeletal dosimetry have shown that increasing the number of micro matrices in the cluster above eight does not change the results for the RBM equivalent dose [12]. However, the effect on the BSC equivalent dose in the 10 μm layer remained unclear because of restrictions with respect to the adequate algorithm and the size of the μCT images available at the time.

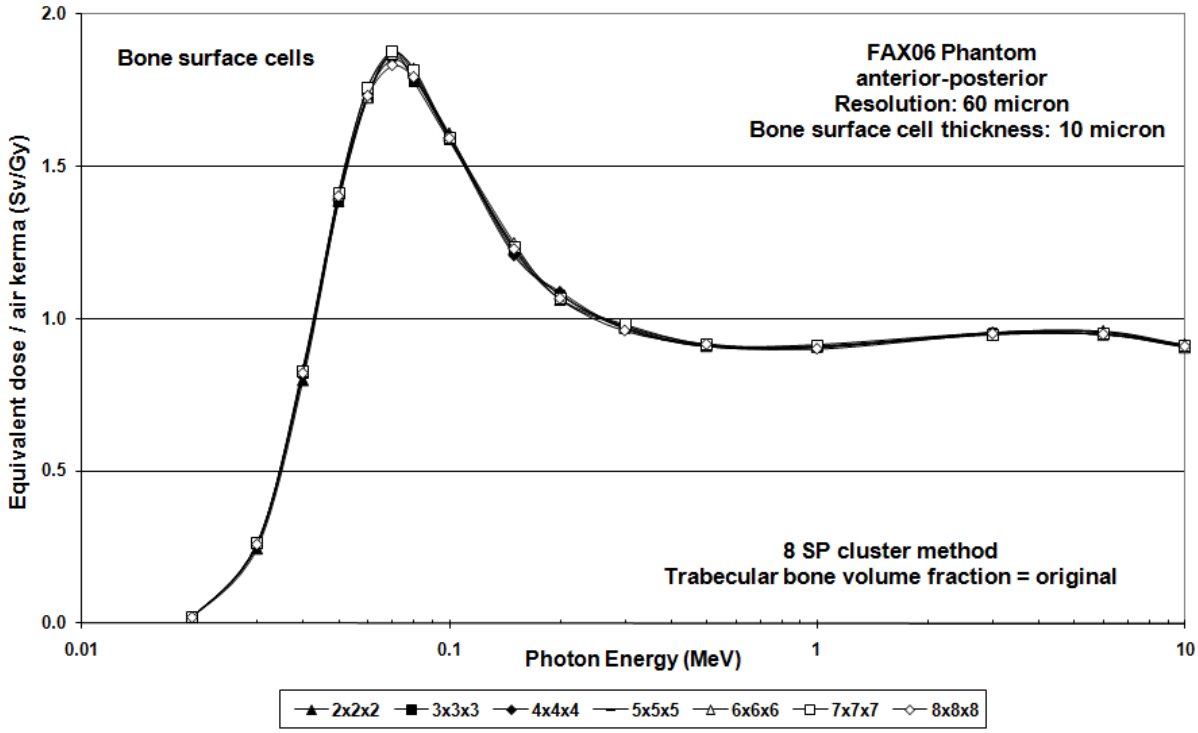

Figure 6. Bone surface cells equivalent dose conversion coefficients for the FAX06 phantom for eight different cluster sizes for anterior-posterior incidence and with original trabecular bone volume fractions.

Figure 6 shows BSC equivalent dose CCs based on 60 μm resolution for the FAX06 phantom, AP incidence and as a function of the incident photon energy for clusters with 2x2x2, 3x3x3, 4x4x4, 5x5x5, 6x6x6, 7x7x7 and 8x8x8 micro matrices. Differences between the CCs can be seen, especially below 200 keV, but the curves are too close to allow for further analysis based on the graph. Therefore, all eight CCs are also shown in table 5 as a function of the incident photon energy.

Increasing the number of micro matrices in the cluster is motivated by the assumption that more coherent microstructure information would automatically improve the quality of the results, i.e. that the BSC equivalent dose would hopefully converge towards an “ideal value” when the number of micro matrices increases. Thus, it is assumed that a larger coherent volume of spongiosa would guarantee better results. If one looks at the BSC equivalent doses in table 5 it is not possible to identify any converging trend when the cluster size increases. One way to examine this more closely is to identify the maximum and minimum values per energy point. The maxima are the bold, italic numbers and the minima are the bold, underlined numbers. They are distributed randomly among all clusters, except for the 8x8x8 cluster, which never shows a maximum value, although it represents the largest coherent spongiosa volume. Consequently, there is no trend, no convergence among these data and the differences found between the CCs are of the same nature as already seen in the previous sections; differences between the trabecular bone structures (= number, form and thickness of the trabeculae) of the clusters are responsible for the differences to be seen between the CCs and correlation with the cluster size or the TBVFs cannot be observed.

Table 5. Bone surface cells equivalent dose conversion coefficients for eight different cluster sizes with original trabecular bone volume fractions

E (MeV)	2x2x2	3x3x3	4x4x4	5x5x5	6x6x6	7x7x7	8x8x8	Max/Min (%)
0.02	0.0207	***0.0218***	0.0210	0.0209	0.0212	**0.0206**	0.0210	5.8
0.03	0.2466	0.2609	0.2574	0.2603	***0.2643***	0.2620	**0.2602**	1.6
0.04	**0.7995**	0.8195	0.8236	***0.8401***	0.8338	0.8278	0.8219	5.1
0.05	1.3879	**1.3822**	1.3927	***1.4139***	1.4076	***1.4139***	1.4017	2.3
0.06	1.7335	1.7260	1.7346	***1.7618***	1.7283	1.7583	1.7311	2.1
0.07	1.8775	1.8771	1.8498	1.8645	1.8706	***1.8791***	**1.8316**	2.6
0.08	1.8085	**1.7797**	1.7942	1.7993	***1.8238***	1.8170	1.7926	2.5
0.1	***1.6099***	**1.5847**	1.5925	1.6039	1.6026	1.5957	1.5925	1.6
0.15	1.2295	1.2393	**1.2079**	1.2166	***1.2509***	1.2371	1.2288	3.6
0.2	1.0819	1.0797	***1.0888***	1.0823	**1.0644**	1.0668	1.0671	2.3
0.3	0.9712	0.9763	0.9689	0.9683	0.9775	***0.9826***	**0.9615**	2.2
0.5	0.9107	0.9120	0.9146	**0.9101**	***0.9183***	0.9166	0.9169	0.9
1.0	0.9088	***0.9161***	0.9077	0.9067	0.9122	0.9091	**0.9019**	1.6
3.0	***0.9566***	0.9554	0.9515	0.9555	0.9505	**0.9484**	0.9517	0.9
6.0	***0.9609***	0.9556	**0.9485**	0.9585	0.9493	0.9498	0.9498	1.3
10.0	***0.9158***	0.9108	0.9153	0.9115	0.9079	**0.9107**	0.9096	0.6

The last column of table 5 shows the percentage difference between the maximum and the minimum BSC equivalent dose per energy point with an average value of 2.3% over all energies. Typically, as seen earlier, these differences are greater for low incident photon energies for the reasons explained in the comments to table 4. Based on the data shown in table 5 it is not possible to identify one specific cluster size as being the best for representing the necessary amount of microstructure information to be used for skeletal dosimetry. Consequently, a cluster with 2x2x2 = 8 micro matrices is sufficient.

The results shown in figure 6 and table 5 have been calculated for a human skeleton with the TBVFs shown in table 1, i.e. TBVFs between 6.67 and 8.32% in all bones. TBVFs can vary considerably among different individuals and among different bone sites. According to ICRP70 [2], typical average adult TBVFs are 10, 12, 15, 20 and 55% for the ribcage, the spine, the long bones, the pelvis and the skull/mandible, respectively. Ideally, one would like to use μCT images of spongiosa from all these bones with exactly the ICRP70-based TBVFs from an adult female or male scanned with the same voxel resolution. Hopefully, the scanning of these five representative bones from one individual with the same voxel resolution will be realized in the near future, although it is improbable that the TBVFs found will be exactly those given by ICRP70.

In the meantime, for the investigation of the minimum number of micro matrices necessary, the gap can be bridged by employing a technique quite common to voxel phantom development: Sometimes digital CT images of a person become available for the construction of a voxel phantom, but then it is found that the resulting organ masses of the segmented images do not correspond to the organ masses recommended by ICRP89 [20]. Then, the organ and tissue volumes can be changed voxel by voxel until the resulting masses match the ICRP89 data. A similar approach, already followed in previous studies [12, 13], was also adopted here to modify the trabecular bone structure of the μCT images until the ICRP70-based TBVFs had been achieved. The modification of the images was performed with an algorithm which uniformly adds/removes trabecular bone micro voxels to/from the trabecular surfaces of the parallelepipeds until the desired TBVF was achieved. Here, in effect the trabecular bone surfaces grow uniformly all over the spongiosa volume until the desired TBVF is reached.

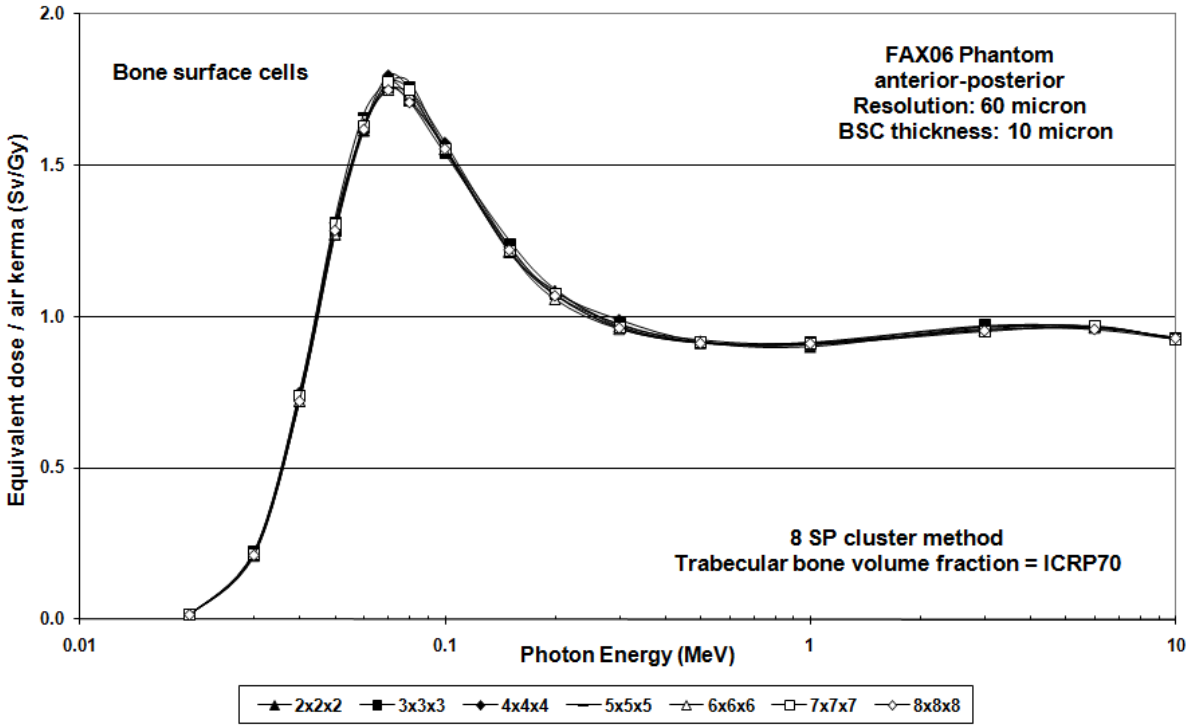

Figure 7. Bone surface cells equivalent dose conversion coefficients for the FAX06 phantom for eight different cluster sizes for anterior-posterior incidence and with ICRP70-based trabecular bone volume fractions.

Table 6. Bone surface cells equivalent dose conversion coefficients for eight different cluster sizes with ICRP70-based trabecular bone volume fractions

E (MeV)	2x2x2	3x3x3	4x4x4	5x5x5	6x6x6	7x7x7	8x8x8	Max/Min (%)
0.02	***0.0174***	0.0168	0.0169	0.0165	0.0159	0.0162	**0.0158**	10.1
0.03	**0.2121**	0.2241	0.2232	***0.2250***	0.2165	0.2163	0.2130	6.1
0.04	0.7223	0.7366	***0.7513***	0.7509	0.7211	0.7373	**0.7220**	4.1
0.05	**1.2720**	1.2832	1.3106	***1.3225***	1.2731	1.3048	1.2870	4.0
0.06	**1.6162**	1.6249	1.6303	***1.6697***	1.6374	1.6301	1.6213	3.3
0.07	1.7726	1.7599	***1.7986***	1.7740	**1.7494**	1.7757	1.7516	2.8
0.08	1.7220	1.7124	1.7550	***1.7744***	1.7370	1.7515	**1.7106**	3.7
0.1	1.5548	**1.5407**	***1.5766***	1.5590	1.5542	1.5535	1.5569	2.3
0.15	**1.2149**	1.2358	1.2338	***1.2520***	1.2172	1.2183	1.2226	3.1
0.2	1.0872	1.0756	1.0835	***1.0911***	**1.0587**	1.0766	1.0708	3.1
0.3	0.9689	0.9779	***0.9912***	0.9729	**0.9600**	0.9627	0.9646	3.3
0.5	0.9160	0.9174	0.9201	***0.9234***	**0.9136**	0.9158	0.9140	1.1
1.0	**0.9022**	***0.9170***	0.9110	0.9129	0.9082	0.9097	0.9130	1.6
3.0	0.9668	***0.9718***	0.9616	0.9666	0.9560	**0.9533**	0.9553	1.9
6.0	0.9684	0.9677	***0.9706***	**0.9571**	0.9642	0.9685	0.9598	1.4
10.0	0.9294	0.9302	**0.9255**	0.9256	***0.9319***	0.9268	0.9307	0.7

Figure 7 and table 6 show BSC equivalent dose CCs based on the ICRP70-based TBVFs. Again, no trend, and no convergence can be identified from the data. As in table 5, maximum and minimum BSC equivalent doses seem to be randomly distributed among the clusters. The percentage differences

between maxima and minima are slightly greater for the ICRP70-based TBVFs with an average value of 3.3% over all energies. This 1% increase is caused by the algorithm which modifies the original TBVFs in order to arrive at the ICRP70-based TBVFs. As observed for the original TBVFs, the data shown in table 6 for the ICRP70-based TBVFs do not justify the selection of one specific cluster as being the best for skeletal dosimetry, which again means that a cluster with 2x2x2 = 8 micro matrices represents a coherent volume of spongiosa sufficient to simulate radiation transport through the trabecular microstructure for a bone-specific distribution of TBVFs.

The technique used here to modify the trabecular bone structure has to be considered as a temporary procedure until μCT images for the above mentioned five bone sites from one individual will become available. On the other hand, the results presented in tables 5 and 6 prove that for the investigation of the minimum number of micro matrices necessary it is not important if the modified trabecular bone structure reflects exactly the real number, form and thickness of the trabeculae of a real specific bone site. Actually, it was shown earlier that even idealized spongiosa made of artificial micro voxels of marrow and trabecular bone would lead to similar results [13].

C. Medullary cortical bone surfaces

Calculations with medullary BSC were performed for both phantoms for AP and PA incidence with the 8 SP cluster method. It was found that the differences between the BSC CCs for the cases with and without medullary BSC were smaller than the range given by the sum of the two statistical errors for all incident photon energies between 10 keV and 10 MeV. This implies that at least for external whole body exposure to photons the inclusion of medullary BSC is dosimetrically not relevant. However, it is possible that this situation may change for partial body exposure of the extremities, as in radiology, and for internal exposures.

IV. CONCLUSIONS

With respect to the questions raised in section I-C, this investigation generated the following results for the exposure conditions considered here:

1) Increasing the voxel resolution of μCT images of spongiosa from 60 to 30 μm had no effect on the RBM equivalent dose, but did influence the BSC equivalent dose. Due to voxel effects, a spongiosa volume scanned at two different resolutions shows slightly different trabecular bone structures (= number, form and thickness of the trabeculae) in the segmented images, which in turn may cause differences between the corresponding BSC equivalent doses for incident photon energies up to 200 keV, here by up to 5%. The reason for this effect is that different fluxes of photoelectrons are released in trabecular bone, which can influence the BSC equivalent dose over a 10 μm distance from the trabecular bone surface, but do not strongly influence the RBM equivalent dose in the marrow cavities with diameters of hundreds of μm.

2) With respect to the minimum amount of microstructure information necessary for the simulation of the trabecular bone structure throughout the spongiosa volume this study has confirmed previous results found for the RBM, now also confirmed for the BSC. During radiation transport calculations, a cluster of 2x2x2 = 8 micro matrices, applied systematically and periodically to the spongiosa voxels of the phantoms, is sufficient to produce BSC equivalent doses consistent with results achieved for clusters with up to 8x8x8 = 512 micro matrices.

3) It was found that the inclusion of BSC on medullary cortical bone surfaces has a negligible effect on the whole body BSC equivalent dose. Differences observed between BSC equivalent doses calculated with and without inclusion of BSC on medullary cortical

bone surfaces were smaller than the combined statistical errors for all incident photon energies. Future studies may show if these findings can also be confirmed for partial body exposures, especially of the extremities, and for internal exposures.

The 8 SP cluster method and the PIRT algorithm mentioned in section I-B are two different MC techniques of skeletal dosimetry, which allow for radiation transport directly in the trabecular microstructure of human spongiosa. Additionally, the 8 SP cluster method can be applied to a complete human skeleton as long as this skeleton has been segmented into cortical bone, spongiosa, medullary YBM and cartilage. For external exposure to photons, this study and the previous investigations [12, 13] have shown that a cluster of only 8 micro matrices extracted from the μCT images and systematically and periodically applied inside the spongiosa volume is suitable to represent the trabecular microstructure environment for the calculation of RBM and BSC equivalent doses.

For incident photon energies below 200 keV, photoelectrons released in bone dominate the electron flux through the spongiosa. When two samples of spongiosa with the same TBVF have different numbers, forms and thicknesses of their trabeculae, then the corresponding photoelectron fluxes reflect these differences, but because of the small range of the photoelectrons entering the marrow cavities, they considerably affect only the equivalent dose to the BSC but not to the RBM. Consequently, for a given TBVF, all RBM equivalent doses presented in this and the previous studies [12-13] are independent of parameters, like the donor of the bone, the bone site, the segmentation method and the voxel resolution, whereas BSC equivalent doses do depend on these parameters. So far, the trabecular bone structure effect on the BSC equivalent dose is less than 5% and it is to be expected that this number will decrease, and may even become smaller than the combined statistical error, if the ICRP will follow a recent proposal to increase the thickness of the bone endosteum from 10 to 50 μm [19], because for a given TBVF, differences of energy deposition caused by different fluxes of trabecular photoelectrons are most relevant in the marrow cavity only very close to the trabecular bone surface. Averaging the energy deposition over a thickness of 50 μm instead of 10 μm will reduce the difference between BSC equivalent doses caused by different trabecular bone structures[13].

This study has shown and confirmed that skeletal dosimetry for external exposure to photons based on μCT images of human spongiosa can be done using a relatively small amount of coherent spongiosa volume extracted from the images. With respect to the consistency of results for the RBM and the BSC equivalent doses one has to be aware of the fact that due to voxel effects ocurring during segmentation, the voxel resolution may particularly influence the BSC equivalent dose; or in more general terms, any equivalent dose in the marrow cavity close to the trabecular bone surface. On the other hand, it would be interesting to find out through future studies, how these percentage effects compare to effects which may be caused by the μCT imaging process itself in case of multiple rescanning, like sample positioning, scanner calibration, etc. Other follow-up projects planned by our research group are the further improvement of segmentation techniques, the segmentation of RBM, YBM and BSC in the marrow cavity at run time and the application of the 8 SP cluster method to skeletal dosimetry for bone-seeking radionuclides.

ACKNOWLEDGMENTS

The authors want to thank Dr. I. Kawrakow from the Ionizing Radiation Standards, National Research Council of Canada, Ottawa, Canada for his assistance with respect to the programming of the EGSnrc-based Monte Carlo code used in this study.
The authors would also like to thank the Conselho Nacional de Desenvolvimento Científico e Tecnológico (CNPq) and the Fundação de Amparo à Ciência do Estado de Pernambuco (FACEPE) for financial support.

REFERENCES

[1] ICRP Limits for Intakes of Radionuclides by Workers (ICRP Publication 30 Oxford: Pergamon 1979)

[2] ICRP Basic Anatomical and Physiological Data for use in Radiological Protection: The Skeleton. (ICRP Publication 70 Oxford: Pergamon 1995)

[3] Jokisch D W, Patton P W, Inglis B A, Bouchet L G, Rajon D A, Rifkin J and Bolch W E "NMR Microscopy of Trabecular Bone and its Role in Skeletal Dosimetry" Health Physics **75**(6), 584-596 (1998)

[4] Jokisch D W, Bouchet L G, Patton P W, Rajon D A and Bolch W E "Beta-particle dosimetry of the trabecular skeleton using Monte Carlo transport within 3D digital images" Med.Phys. **28** (7), 1505-1518 (2001)

[5] Bolch W E, Patton P W, Rajon D A, Shah A P, Jokisch D W and Inglis B A "Considerations of Marrow Cellularity in the 3-Dimensional Dosimatric Models of the Trabecular Skeleton" J Nucl Med **43**, No.1, 97- 108 (2002)

[6] Patton P W, Rajon D A, Shah A P, Jokisch D W, Inglis B A and Bolch W E "Site-specific variability in trabecular bone dosimetry: Considerations of energy loss to cortical bone" Med.Phys. **29** (1), 6-14 (2002)

[7] Rajon D A, Jokisch D W, Patton P W, Shah A P, Watchman C J and Bolch W E Voxel effects within digital images of trabecular bone and their consequences on chord-length distribution measurements Phys.Med.Biol. **47** 1741-1759 (2002)

[8] Shah A P, Bolch W E, Rajon D A, Patton P W and Jokisch D W "A Paired-Image Radiation Transport Model for Skeletal Dosimetry" J Nucl Med **46**, No.2, 344-353 (2005)

[9] Shah A P, Rajon D A, Patton P W, Jokisch D W and Bolch W E "Accounting for beta-particle loss to cortical bone via paired-image radiation transport (PIRT)" Med.Phys. **32** (5), 1354-1366 (2005)

[10] Nelson W R, Hirayama H and Rogers D W O "The EGS4 Code System" *SLAC-265*, Stanford Linear Accelerator Center, Stanford University, Stanford, CA,USA (1985)

[11] Kawrakow I "Accurate condensed history Monte Carlo simulation of electron transport. I. EGSnrc, the new EGS4 version", Med.Phys. **27**, 485-498 (2000)

[12] Kramer R, Khoury H J, Vieira J W and Kawrakow I "Skeletal dosimetry in the MAX06 and the FAX06 phantoms for external exposure to photons based on vertebral 3D-microCT images" Phys.Med.Biol. **51** 6265-6289 (2006)

[13] Kramer R, Khoury H J, Vieira J W and Kawrakow I "Skeletal dosimetry for external exposure to photons based on μCT images of spongiosa from different bone sites" Phys.Med.Biol **52** 6697-6716 (2007)

[14] Kawrakow I Accurate condensed history Monte Carlo simulation of electron transport. II. Application to ion chamber response simulations, *Med.Phys.* **27**, 499-513 (2000)

[15] Kawrakow I and Rogers D.W.O. "The EGSnrc code system: Monte Carlo simulation of electron and photon transport", NRC Report PIRS-701 (2003)

[16] Kawrakow I "Version V4-r2-2-3 of the EGSnrc code system" *http://www.irs.inms.nrc.ca/EGSnrc/EGSnrc.html* (2006)

[17] Kramer R, Khoury H J, Vieira J W and Lima V J M "MAX06 and FAX06: Update of two adult human phantoms for radiation protection dosimetry" Phys. Med. Biol. **51** 3331-3346 (2006)

[18] SCION Image for WINDOWS, Scion Corporation, www.scioncorp.com (2000)

[19] Bolch W E, Shah A P, Watchman C J, Jokisch D W, Patton P W, Rajon D A, Zankl M, Petoussi-Henss N and Eckerman K F "Skeletal Absorbed Fractions for Electrons in the Adult Male: Considerations of a Revised 50-μm Definition of the Bone Endosteum" Rad.Prot.Dos. **127** 169-173 (2007)

[20] ICRP Basic Anatomical and Physiological Data for Use in Radiological Protection: Reference Values (ICRP Publication 89 Oxford: Pergamon 2002)